Wall Layer Formation in Continuously Operated Tubular Reactors for Free-Radical Polymerizations

Stefan Welzel*, Christian Zander, and Ulrich Nieken

Supporting Information available online

Polymer fouling is a major problem for the operation of continuous reactors. Therefore, it is important to understand and quantitatively describe the mechanisms leading to formation of fouling deposits. In this work, a CFD model for the radical polymerization of N-vinylpyrrolidone is presented, where the reaction kinetics, a viscosity model, and a transport model for polymer moments are determined from independent experiments. The model is compared to experimental obtained residence time distributions in capillary reactors over a wide range of concentrations. Model predictions are in good agreement with experimental findings.

Keywords: Fouling in continuous reactors, N-vinylpyrrolidone, Radical polymerization, Wall layer

1 Introduction

Batch or semi-batch operated tank reactors are the primary means of producing specialty polymers like polyvinylpyrrolidone (PVP). The key benefit of this process type is its high flexibility. Continuously operating reactor systems have been taken into consideration in the context of process intensification due to increased controllability, greater energy efficiency, and improved heat transfer. To create low-volume products like PVP, tubular reactors with mixing elements are of interest. Appearance of fouling deposits in continuously operating mixer-reactors that cause blocking and shutdown are a major drawback for the polymerization of N-vinylpyrrolidone (NVP). Fig. 1 shows a mixing element, which is completely covered with fouling deposits. During polymerization, these deposits accumulate over time until total blocking. Accordingly, the pressure in the reactor rises until a shutdown is unavoidable. Fouling is predicated on side reactions that result in large molecular weight, branching, or even crosslinked polymer chains. Increased local residence time and sluggish flow in dead zones promote the creation of a polymer network [1–3]. To optimize process conditions and predict fouling during reactor scale-up, it is necessary to understand the causes of deposit formation and derive a model that allows to describe the growth of a deposit layer. Starting with the simplest continuous reactors: the tubular capillary reactors.

The reaction mechanism of NVP polymerization has been studied extensively [1, 4–8]. In a prior study, the primary cause of long chain branching was found to be the production of terminal double bonds (TDBs) by transfer to monomers and subsequent propagation [9]. Then, models to describe the number of terminal double bonds was developed and validated against experimental data from a CSTR reactor [10]. In a recently published work, those models were extended to describe the branching point distribution [11]. Therefore, the reaction mechanism is only briefly discussed in this work.

A polymer distribution is usually represented by its moments. Thus, to calculate transport in a polymer system, a formulation for the transport of moments of the polymer is needed. This is only possible if the moments close or if there is a suitable closing condition. To archive this, two simplifications of the Stefan-Maxwell diffusion were derived, which convert the transport equation of polymeric species to a closed set of transport equations for the polymer moments. The first approach corresponds to an infinitely diluted polymer system, whereas the second one describes a highly concentrated polymer system [12–14]. Both formulations were compared with the full Stefan-Maxwell model of a ternary mixture of a solvent and two polymer species of different chain length. This paper describes the two approaches and shows why the approach for

[1]Stefan Welzel ⬤ https://orcid.org/0000-0002-8842-0485 (stefan.welzel@icvt.uni-stuttgart.de), [1]Dr.-Ing. Christian Zander, [1]Prof. Ulrich Nieken

[1]University of Stuttgart, Institute of Chemical Process Engineering, Boeblingerstrasse 78, 70199 Stuttgart, Germany.
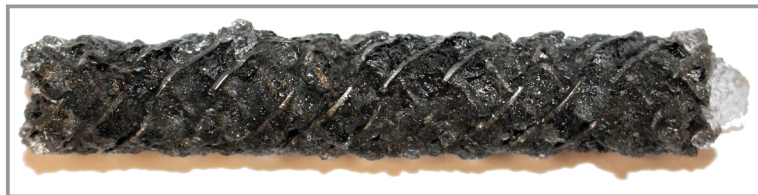
Figure 1. Fouling deposits in a static mixing element after the operation of N-vinylpyrrolidone in a Fluitec® ContiPlant reactor.

concentrated polymer solutions was used to further investigate the formation of wall layers.

The kinetic model and the transport model for polymers are then implemented together with a viscosity model in an in-house developed CFD solver. The CFD model can be used to describe the wall layer formation and is later validated by experimental findings in the capillary reactor for a wide range of concentrations.

2 Experimental Details

2.1 Chemicals

N-vinylpyrrolidone stabilized with 0.5 % NaOH was supplied by BASF SE and was purified by distillation under vacuum to remove stabilizer and high-molecular compo-

nents directly before the experiments. Initiator (V-50, Wako Chemicals) was stored in the refrigerator and used as delivered. Deionized water has been used as solvent.

2.2 Experimental Setup

To gain insight into the mechanism of the formation of fouling, we need to determine the buildup of the wall layer. A reaction system with capillary tubular reactors has been set up, where the residence time distributions at different times of the reaction can be recorded. In Fig. 2 the simplified flow sheet for the reaction system is shown. Two storage containers were prepared, one containing a mixture of monomer and solvent, the other containing initiator dissolved in the solvent. Both containers were degassed under vacuum. The feed streams were pumped by two Knauer HPLC piston pumps and controlled by employing Bronkhorst Coriolis mass flow meters and PI controllers. The feed streams from both tanks were mixed in a 1:1 ratio by using a dynamic mixing chamber (Knauer Wissenschaftliche Geräte GmbH) at room temperature to ensure good mixing quality before entering the reactor. A HPLC switching valve (two position microelectric valve actuator (8 ports) by VICI Valco Instruments Co. Inc.) is used to pulse a tracer solution in the reaction medium.
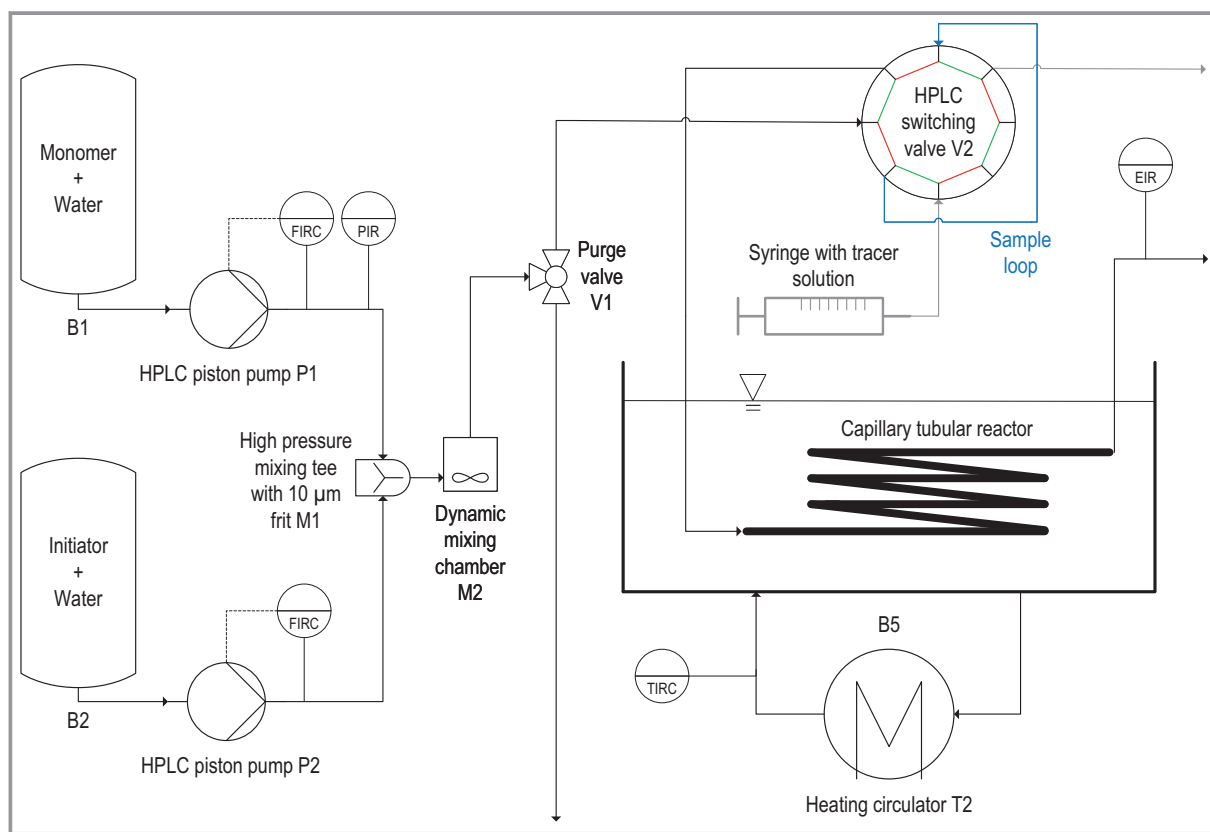

Figure 2. Simplified flow sheet for the reaction system for the polymerization of N-vinylpyrrolidone.

NaCl solution (1 M) was used as a tracer. The capillary tubular reactor (stainless steel 1.4435 by Swagelok Company) is then placed in a tempered oil bath (VWR) to conduct polymerizations at a temperature of $T = 85\,°C$. At the end of the reactor a conductivity measurement with a flow-thru conductivity electrode (ET908 with 93 µl of eDAQ Pty Ltd) is conducted. With this setup a formation of a wall layer can be observed by measuring the residence time distribution.

3 CFD Model

To model the formation of a wall layer, all the influencing mechanisms, which are shown in Fig. 3, need to be considered. Due to polymerization reactions, the polymer weight fraction increases along the reactor axis. Accordingly, the viscosity increases substantially causing the diffusive transport of the polymers to decrease. In turn, average residence time increases, especially in areas close to the wall. For this reason, the concentration gradients increase, resulting in mass transport perpendicular to the flow field. All these mechanisms are interdependent and cause the formation of a wall layer. Therefore, the goal is to describe these mechanisms with a capable model.

Fig. 4 shows an overview of the developed CFD model, which was implemented in an OpenFOAM environment. Besides solving the momentum and component balances, the reaction kinetics were implemented in a moment model of the polymer distribution. The concentration dependence of viscosity is accounted for using a correlation depending on polymer weight fraction and average molecular weight. In addition, we developed a new mass transport model for polymer moments derived from limiting cases of Stefan-Maxwell diffusion. A detailed description of the model equations for the CFD model can be found in the Supporting Information.
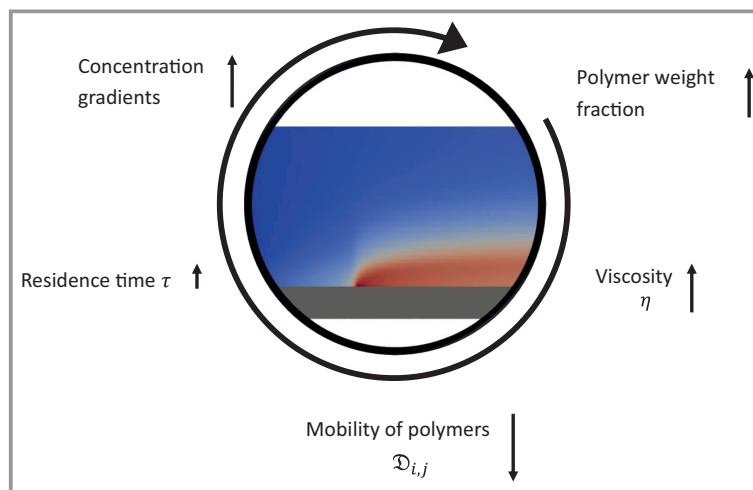

Figure 3. Influencing factors of the wall layer formation in capillary tubular reactors.

tion, propagation and termination by combination, the transfer to monomer and subsequent propagation of TDB reaction are important side reactions for the formation of branching points [10, 11].

Fig. 5 shows two important side reactions. The transfer to monomer reaction leads to a monomer molecule with a terminal double bond. If this monomer molecule propagates further and terminates, a dead polymer species with a terminal double bond is formed. This dead polymer containing terminal double bonds can subsequently react with a living chain because of the terminal double bond and form a branching point. If further reactions with chains containing terminal double bonds take place, highly branched or crosslinked polymer molecules are created.

The kinetic model was validated in terms of monomer conversion, average molecular weight and molecular weight distribution in a CSTR reactor [10].

The reaction mechanism results in a multidimensional property distribution. Since a three-dimensional distribution

3.1 Reaction Kinetics

The reaction scheme for the radical polymerization of N-vinylpyrrolidone was identified in [9] and is summarized in Tab. 1. The dead species are defined as P, and the living species are defined as R. Three different property coordinates are taken into account: chain length (n,m), number of terminal double bonds (i,j), and number of branching points (k,l). Besides classical reactions for a radical polymerization like initia-
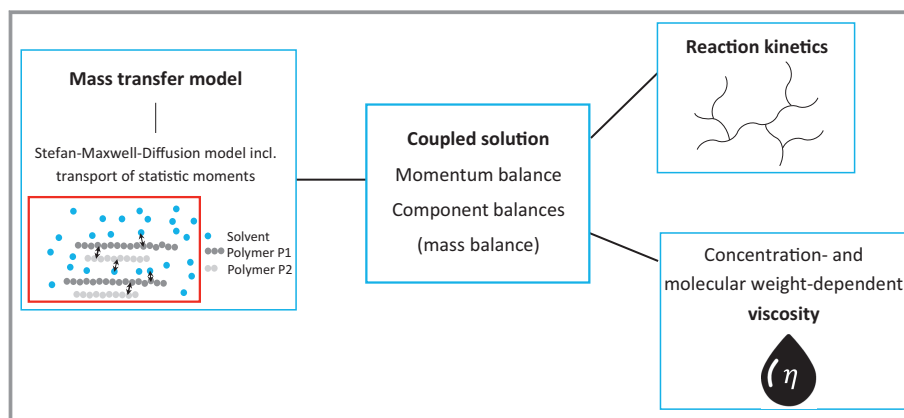

Figure 4. Overview about the developed CFD model with implemented reaction kinetics, concentration and molecular weight-dependent viscosity and a mass transfer model.

Table 1. Set of reactions for the polymerization of N-vinylpyrrolidone in aqueous solution with the chain length (n,m), the number of terminal double bonds (i,j) and the number of branching points (k,l) [9].

Initiator dissociation/ Initiation	$I_2 \xrightarrow{k_d, f_d} 2I / I + M \xrightarrow{k_p} R_{1,0,0}$
Propagation	$R_{n,i,k} + M \xrightarrow{k_p} R_{n+1,i,k}$
Termination by recombination	$R_{n,i,k} + R_{m,j,l} \xrightarrow{k_{t,c}} P_{n+m,i+j,k+l}$
Transfer to monomer	$R_{n,i,k} + M \xrightarrow{k_{tr,M}} P_{n,i,k} + R_{1,1,0}$
Propagation of terminal double bonds	$R_{n,i,k} + P_{m,j,l} \xrightarrow{j \cdot k_{p,TDB}} R_{n+m,i+j-1,k+l+1}$

is practically impossible to solve, the system must be reduced. For the implementation in a CFD model, a zero-dimensional kinetic model is useful since it drastically reduces the computation time. For this purpose, the "TDB double moment model" developed in [10] is used. The branching coordinate was neglected here since it has no impact on the reaction kinetics. Subsequently, the method of "pseudodistributions" or "distributed counters" was applied for the number of terminal double bonds and for the chain length, respectively. The method of moments calculates mathematical mean values for the respective property coordinates.

3.2 Viscosity Correlation

The viscosity has a very large influence on the formation of the surface layer in continuous tubular reactors. To correctly represent the formation of the surface layer the dependence of viscosity on polymer weight fraction w_P and average molecular weight MW must be accounted for. This can be achieved by using Huggin's equation [15]

$$\eta = \eta_{ref}\left(1 + [\eta]w_P + k_H[\eta]^2 w_P^2\right) \qquad (1)$$

with the reference viscosity $\eta_{ref} = 1.02$ mPa s and the constant k_H. In combination with the Mark-Houwink equation

$$[\eta] \propto MW^\alpha \text{ with } \alpha = 0.5 - 0.8 \qquad (2)$$

a relation of viscosity on polymer weight fraction and molecular weight can be formulated

$$\eta = \eta_{ref}\left(1 + k_1 w_P MW^\alpha + k_2 (w_P MW^\alpha)^2\right) \qquad (3)$$

After a series expansion to the complete virial equation [15], it follows

$$\eta = \eta_{ref}\left(1 + \sum k_j (w_P MW^\alpha)^j\right) \qquad (4)$$

Since the free radical polymerization of N-vinylpyrrolidone is investigated at $T = 85\,°C$, viscosity measurements of different PVP blends (K12, K30, K90) were performed only at this temperature and parameters are fitted. The measurements were carried out on a rheometer (MCR 302, Anton Paar GmbH, Graz, Austria) in the shear rate range from $0.1\,s^{-1}$ to $100\,s^{-1}$. A cylinder geometry with a diameter of 27 mm was used. Six points per decade were recorded with a measurement point duration of 20 s. For the highly viscous samples, a cylinder geometry with a diameter of 11 mm was used. To prevent evaporation of the sample the samples were coated with a thin layer of low-viscosity kerosene oil before starting the measurement. Through these measurements it is possible to perform a parameter fit. The scatter of k_1 can be reduced by using a three-term equation [15]. The correlation is given in Eq. (5).
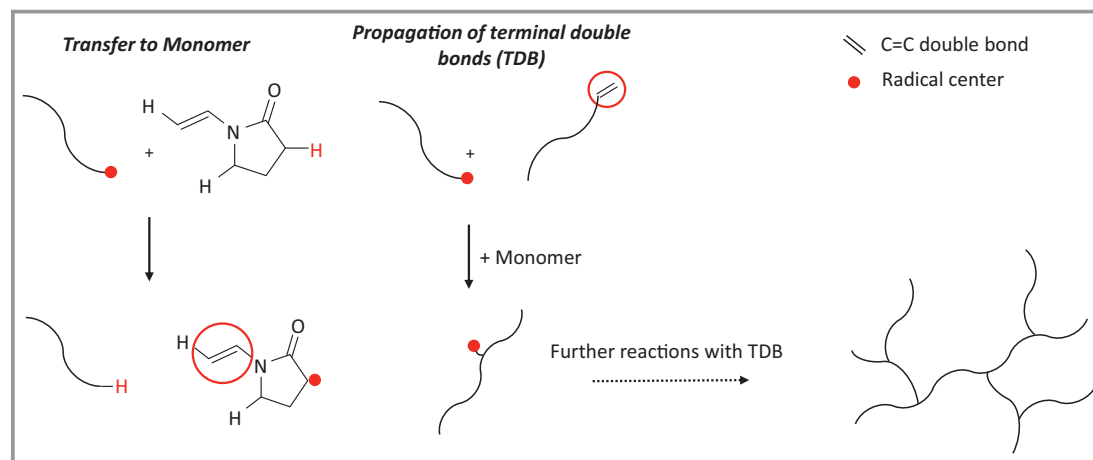

Figure 5. Side reactions (transfer to monomer and subsequent propagation of terminal double bonds reaction) leading to highly branched polymers.

$$\eta(@85\,°C) = \eta_{ref} \left(\begin{array}{l} 1 - 1.503 \left(\dfrac{w_P}{0.2} \left(\dfrac{MW}{5e5\frac{g}{mol}} \right)^{0.3765} \right) \\[2mm] +103.3 \left(\dfrac{w_P}{0.2} \left(\dfrac{MW}{5e5\frac{g}{mol}} \right)^{0.3765} \right)^{3} \\[2mm] +45.35 \left(\dfrac{w_P}{0.2} \left(\dfrac{MW}{5e5\frac{g}{mol}} \right)^{0.3765} \right)^{8} \end{array} \right) \qquad (5)$$

The parity plot in Fig. 6 shows the validity of the correlation and shows very good agreement between predicted and experimentally determined values.
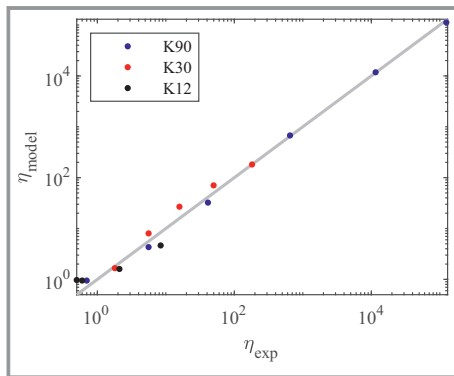

Figure 6. Parity plot of the measured and predicted viscosities for different K-values.

3.3 Mass Transfer Model

The diffusive transport for polymers changes with viscosity and chain length. In CFD calculations the treatment of an infinite number of polymer species is infeasible. Instead of solving the balance equation for each polymer species only the statistical moments of the chain length distribution are calculated.

While the convective transport of polymer species can be converted to moments transport directly, this is not the case for diffusive transport. Balance equations of polymer moments require moment closure or application of a closure condition.

To describe the interactions between polymer and solvent, we start from the Stefan-Maxwell diffusion approach [16]

$$d_i = \frac{x_i}{RT}\nabla\mu_i = -\sum_{j=1}^{n} \frac{x_i x_j (v_i - v_j)}{\mathfrak{D}_{ij}}$$

$$= -\sum_{j=1}^{n} \frac{x_i J_i^N - x_j J_i^N}{c\mathfrak{D}_{ij}} \qquad (6)$$

with the driving force d_i, the mole fractions x_i the universal gas constant R, the temperature T, the chemical potential μ_i,

the total number of components n, the component velocity v_i, the Stefan-Maxwell diffusion coefficient $\mathfrak{D}_{ij}$, the molar diffusive flux J_i^N relative to a mole-averaged velocity (indicated by upper index N) and the total concentration c.

Each sum term describes the friction between two different species. A simple way to obtain a closed expression would be to take a single constant diffusion coefficient between solvent and polymer species and between polymer species of different chain length. In this case, however, the transport of the polymers would be greatly overestimated. With a choice of different diffusion coefficients, no closure for the moments for the Stefan-Maxwell diffusion can be obtained.

For this reason, a closer look at the two limiting cases for Stefan-Maxwell diffusion have been examined [16]. An overview about model assumptions is depicted in Fig. 7. The basic assumption of the first limiting case is a highly diluted polymer solution. This allows to assume for an infinite diffusion coefficient between polymer chains which corresponds to neglection of friction between them. For a better explanation a 3-component system is shown in Fig. 8. Solvent is depicted as blue dots, two polymers, denoted as P1 and P2, of the same type but with different chain length. The friction between polymer chains is completely neglected and only friction between the polymer chain and solvent (or monomers) is considered.

With this assumption, a moment closure can be achieved and an expression for diffusive transport of higher moments is obtained. Assuming additionally for an ideal mixture we term this limiting case "No Polymer Friction model". The diffusive fluxes of statistical moments $J_{\xi^k}^N$ can be calculated from

$$J_{\xi^k}^N = \sum_{s=1}^{\infty} s^k J_{P(s)}^N = \sum_{j=1}^{n_{low}} \frac{\xi^k J_j^N - \mathfrak{D}_P \left(c\nabla\xi^k - \xi^k\nabla c \right)}{c_j} \qquad (7)$$

with the number of chains s, the diffusion coefficient between polymer and low molecular species $\mathfrak{D}_P$, the concentration of low molecular species c_j, n_{low} the total number of low molecular species, the kth chain length moment ξ^k and the flux of low molecular species J_j^N [16].
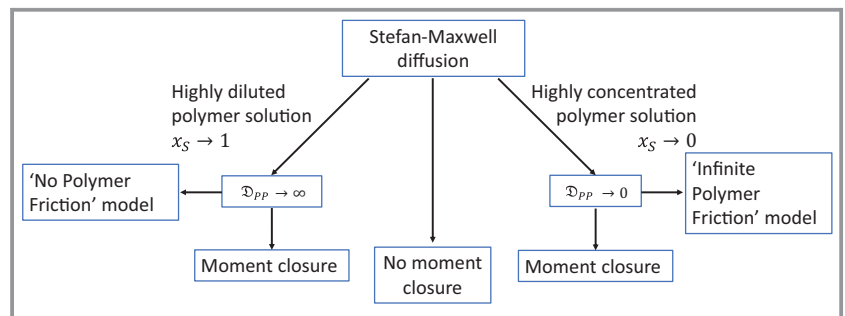

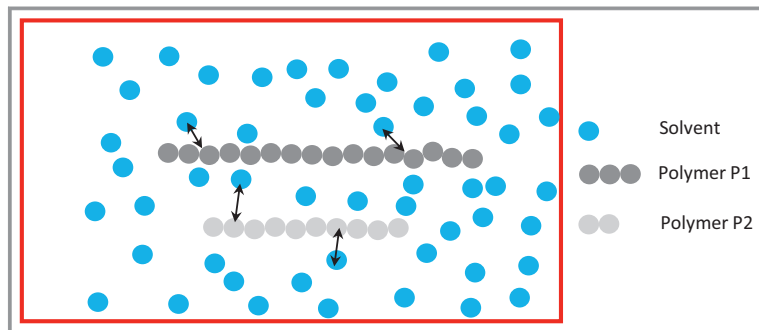**Figure 7.** Overview of the Stefan-Maxwell diffusion with the two limiting cases [16].

Figure 8. Visualization of the "No Polymer Friction" model. The arrows illustrate the interaction of the species.

preserves the polymer's spatial inhomogeneities and exhibits a realistic physical behavior for concentrated polymer solutions. Physical consistency is also maintained because, regardless of the degree of the polymer moment, all polymer moments have the same species velocity.

The Stokes-Einstein relation served as the inspiration for scaling the Maxwell-Stefan diffusion coefficients by η_{rel}

$$\mathfrak{D}_{0/P} = \frac{\mathfrak{D}^0_{0/P}}{\eta_{rel}} \qquad (9)$$

with the reference Maxwell-Stefan diffusion coefficient $\mathfrak{D}^0_{0/P}$ for $w_P \to 0$ to include the effect of decreasing diffusion coefficients with increasing solution viscosity. $\mathfrak{D}_0$ denotes the diffusion coefficient between two low molecular species. Diffusion coefficients are influenced by concentrations as well as the length of the polymer chain. An estimate for the ratio

$$\frac{\mathfrak{D}_P}{\mathfrak{D}_0} = \left(\frac{\xi^1}{\xi^0}\right)^{-0.6} \qquad (10)$$

was inspired by the Zimm theory. However, this approximation can only be rough because the latter was developed for monodisperse, linear polymers in diluted solution.

In special cases like regions of low convective transport (i.e., behind mixing elements) or polymer fouling close to walls of micro reactors, the assumptions of the "No Polymer Friction" model introduces large errors [16]. This is especially true at high polymer content. In this case we propose a second limiting case of the Stefan-Maxwell model, where we assume that friction between polymer chains is very high. This is equivalent to the limit that all binary Stefan-Maxwell diffusion coefficients between polymer chains of different lengths approach zero. For a better explanation the same 3-component system is shown in Fig. 9 again. The friction between the polymer chains P1 and P2 is so high that they only move together relative to the solvent. This means that the diffusive flux of the polymers P1 and P2 is coupled.

Herewith a closure for polymer moments is possible. Finally, we obtain an expression for the transport of higher moments for this limiting case (denoted as "Infinite Polymer Friction model") which depends on the transport of the 0th moment [16]

4 Results and Model Validation

To validate the model, experimental results from the capillary reactor are compared with simulations over a wide concentration range. Subsequently, simulations of deposit formation are discussed in detail.

4.1 Geometry and Boundary Conditions

The reactor has a total length of 3 m and an inner diameter of 1.76 mm. For comparison 3D simulations have been conducted by using a wedge geometry. The initial conditions are previous calculated plug flow solutions for numerical reasons. The inlet velocity was chosen the same as in the experiments to 12 mm s^{-1} and the feed concentrations as well from 5–20 wt % monomer and 0.002–0.02 wt % initiator. This corresponds to an average residence time of 250 s and a monomer conversion between 15–50 % depending on monomer and initiator concentration. A total reaction time of 100 min at temperature of $T = 85\,°C$ was simulated. The remaining parameters for the reference case for the simulations are defined in Tab. 2.

$$J^N_{\xi^k} = \frac{\xi^k}{\xi^0} J^N_{\xi^0} \qquad (8)$$

This equation is also valid for any descriptions of the chemical potential. Higher moments will not equilibrate if the total concentration of polymers remains constant. This
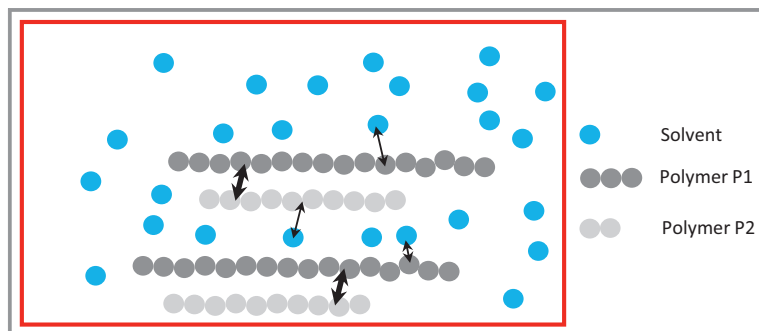

Figure 9. Visualization of the "Infinite Polymer Friction" model. The arrows illustrate the interaction of the species.

Table 2. Reference set of parameters for the simulations.

| Parameter	Reference value
Reference viscosity η_{ref} [Pa s]	$1.02 \cdot 10^{-3}$
Diffusion coefficient between low molecular species $\mathfrak{D}_0^0$ [m^{2}s^{-1}]	$5 \cdot 10^{-9}$
Quotient of the diffusion coefficient between polymer and low molecular species and the coefficient between low molecular species $\mathfrak{D}_P/\mathfrak{D}_0$	0.014
Monomer density ρ_M^0 [17] [kg m^{-3}]	989.72
Solvent density ρ_S^0 [17] [kg m^{-3}]	958.57
ρ_j^0 (all other) [kg m^{-3}]	1200
Molecular weight of monomer MW_M [kg mol^{-1}]	0.1114
Molecular weight of initiator MW_{I2} [kg mol^{-1}]	0.2712
Molecular weight solvent MW_S [kg mol^{-1}]	0.0180

4.2 Model Validation

Fig. 10 shows the comparison of the residence time distribution (RTD) for the experiments and simulations for different monomer concentrations. In Fig. 10A the RTD with feed concentration of monomer of 20 wt % is shown. The residence time distribution of water is plotted as reference. Furthermore, tracer injections were made after 2, 15, 30 and 60 min after start of polymerization. It can be seen that the time for breakthrough shortens over time on stream while

the tailing increases. The reason is the formation of a highly viscous wall layer. Due to cross section narrowing, the breakthrough of the tracer shifts to shorter times and tailing increases due to reduced transport in the viscous wall layer. Simulated residence time distributions show the same trends. Fig. 10B shows the residence time distributions for a lower monomer concentration of 5 wt %. The tends are less pronounced compared to higher monomer concentrations but it is clearly visible. Again, the simulated RTDs are again in good agreement to the experimental data. Fig. 10C shows a case where the initiator concentration is 10 times lower compared to case A (0.002 wt % instead of 0.02 wt %) The breakthrough of the tracer occurs slightly faster, and the tailing is less pronounced for higher times. As with lower monomer concentration, a lower initiator concentration also results in smaller wall deposits. In all cases simulations are in qualitatively good agreement with the experimental findings and general trends are good predicted. The tailing of the distributions in the experiments is more pronounced as in the simulations. We attribute this to transport properties of the tracer in the wall layer, which was only estimated.

4.3 Simulation Results

To gain a better understanding of the formation of the wall layer, the relative viscosity η_{rel} and polymer weight fraction w_p is shown in Fig. 11 for 22 min and 100 min time on stream. After 22 min a viscous wall layer is formed at a certain distance to the reactor entrance, which exhibits a high polymer weight fraction. This wall layer grows uniformly up to the reactor outlet. Over time polymer content of the
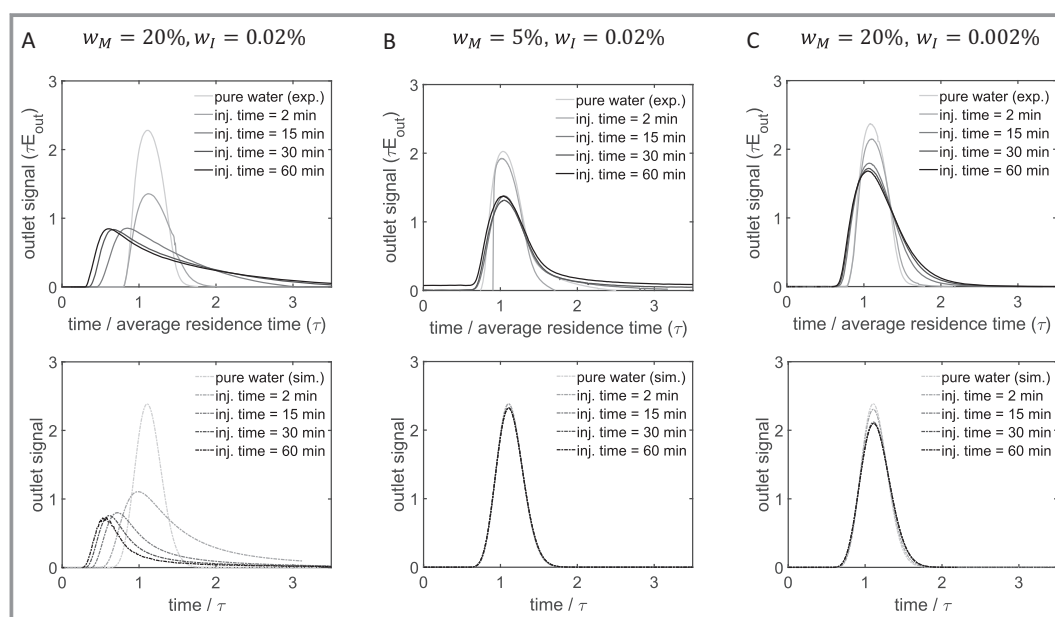
Figure 10. Residence time distributions for experiments (top) and simulations (bottom) for different monomer and initiator concentrations.
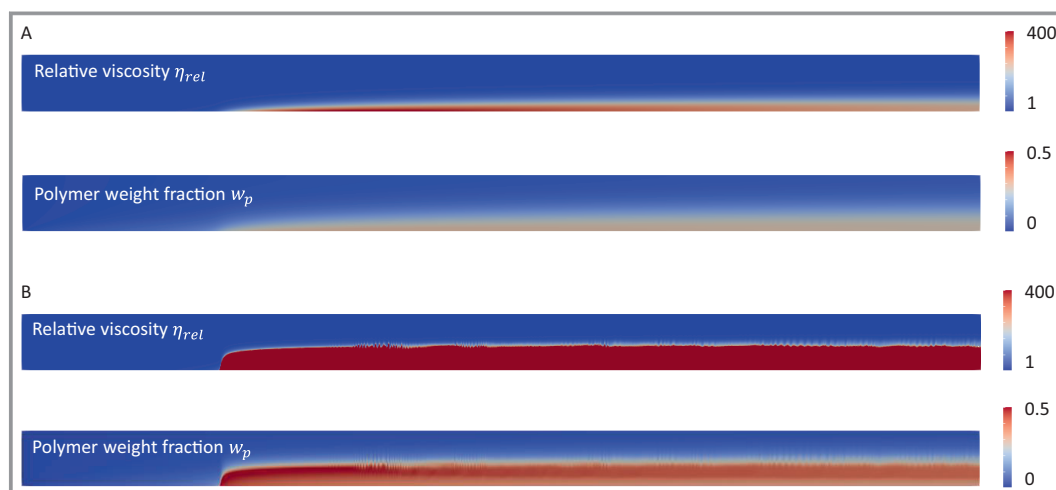
Figure 11. Simulation results for the relative viscosity η_{rel} and the polymer weight fraction w_P for two different times (A: 22 min and B: 100 min reaction time) for a monomer concentration of $w_M = 20$ wt % and an initiator concentration of $w_I = 0.02$ wt %.

layer increases to $w_P = 0.5$ (100 min), much higher than average conversion.

5 Conclusion

A CFD model was developed to simulate the formation of a highly viscous wall layer during free radical polymerization on N-vinylpyrrolidone. The reaction kinetics, a concentration- and molecular weight-dependent correlation for the viscosity and a new mass transport model for the transport of statistical polymer moments were derived and implemented in the CFD model. Starting from the full Stefan-Maxwell approach two limiting cases of the Stefan-Maxwell diffusion model were derived, which allow closure of diffusive transport in terms of moments. For wall layer formation the "Infinite Polymer Friction" model is well suited to model areas close to the wall since the polymer content is high. To validate the CFD model, a capillary reactor was set up to track the formation of a highly viscous wall layer by residence time measurements. The simulations coincide with experimental findings over a wide range of operation conditions.

Supporting Information

Supporting Information for this article can be found under DOI: https://doi.org/10.1002/cite.202200195.

Acknowledgment

Greek letters

ξ^k	[–]	k^{th} Moment
α	[–]	Fitting factor
η	[Pa s]	Dynamic viscosity
ρ	[kg m^{-3}]	Density
τ	[s]	Residence time

Sub- and Superscripts

I	Initiator
i,j	Number of terminal double bonds
i,j	Species i,j
k,l	Number of branching points
M	Monomer
n,m	Chain length
P	Polymer
Ref	Reference
S	Solvent

Abbreviations

CFD	Computational Fluid Dynamics
CSTR	Continuous stirred tank reactor
HPLC	High pressure liquid chromatography
I	Initiator
Inj.	Injection
M	Monomer
NVP	N-Vinylpyrrolidone

P	Dead polymer species
P1	Polymer 1
P2	Polymer 2
PI	Proportional Integral
PVP	Polyvinylpyrrolidone
R	Living polymer species
RTD	Residence time distribution
TDB	Terminal double bond
V50	2,2'-azobis(2-methylpropionamidine) dihydrochloride

References

[1] J. Urrutia, A. Peña, J. M. Asua, *Macromol. React. Eng.* **2017**, *11 (1)*, 1–14. DOI: https://doi.org/10.1002/mren.201600043

[2] D. Kohlmann et al., *Macromol. React. Eng.* **2016**, *10 (4)*, 339–353. DOI: https://doi.org/10.1002/mren.201500079

[3] C. Bernstein, *Methoden zur Untersuchung der Belagsbildung in chemischen Reaktoren*, Dissertation, Universität Hamburg **2017**.

[4] M. Stach, I. Lacík, D. Chorvát, M. Buback, P. Hesse, R. A. Hutchinson, L. Tang, *Macromolecules* **2008**, *41 (14)*, 5174–5185. DOI: https://doi.org/10.1021/ma800354h

[5] L. Uhelská, D. Chorvát, R. A. Hutchinson, S. Santanakrishnan, M. Buback, I. Lacík, *Macromol. Chem. Phys.* **2014**, *215 (23)*, 2327–2336. DOI: https://doi.org/10.1002/macp.201400329

[6] J. Schrooten, M. Buback, P. Hesse, R. A. Hutchinson, I. Lacík, *Macromol. Chem. Phys.* **2011**, *212 (13)*, 1400–1409. DOI: https://doi.org/10.1002/macp.201100021

[7] S. Santanakrishnan, L. Tang, R. A. Hutchinson, M. Stach, I. Lacík, J. Schrooten, P. Hesse, M. Buback, *Macromol. React. Eng.* **2010**, *4 (8)*, 499–509. DOI: https://doi.org/10.1002/mren.201000007

[8] F. Haaf, A. Sanner, F. Straub, *Polym. J.* **1985**, *17 (1)*, 143–152. DOI: https://doi.org/10.1295/polymj.17.143

[9] P. Deglmann, M. Hellmund, K. Hungenberg, U. Nieken, C. Schwede, C. Zander, *Macromol. React. Eng.* **2019**, 1900021. DOI: https://doi.org/10.1002/mren.201900021

[10] C. Zander, K. D. Hungenberg, T. Schall, C. Schwede, U. Nieken, *Macromol. React. Eng.* **2020**, *14 (3)*, 2000009. DOI: https://doi.org/10.1002/mren.202000009

[11] S. Welzel, C. Zander, K. Hungenberg, U. Nieken, *Macromol. React. Eng.* **2022**, *16 (4)*, 2200005. DOI: https://doi.org/10.1002/mren.202200005

[12] C. Zander, *Fouling during solution polymerization in continuously operated reactors*, Dissertation, Universität Stuttgart **2021**.

[13] W. Säckel, U. Nieken, in *Process-Spray*, Springer International Publishing, Cham **2016**.

[14] W. Säckel, U. Nieken, *Chem. Ing. Tech.* **2014**, *86 (4)*, 438–448. DOI: https://doi.org/10.1002/cite.201300148

[15] D. W. Van Krevelen, K. Te Nijenhuis, *Properties of Polymers*, Elsevier, Amsterdam **2009**.

[16] S. Welzel, W. Säckel, U. Nieken, *Macromol. React. Eng.* **2022**, 2200045. DOI: https://doi.org/10.1002/mren.202200045

[17] S. Santanakrishnan, L. Tang, R. A. Hutchinson, M. Stach, I. Lacík, J. Schrooten, P. Hesse, M. Buback, *Macromol. React. Eng.* **2010**, *4*, 499–509. DOI: https://doi.org/10.1002/mren.201000007